Operation Under Fault Conditions of the Stacked Polyphase Bridges Converter

Mojgan Nikouie[1], Oskar Wallmark[1], Lennart Harnefors[12], Hans-Peter Nee[1]
[1]Department of Electric Power and Energy Systems,
KTH Royal Institute of Technology, 100 44 Stockholm, Sweden
[2]ABB, Corporate Research, 721 78 Västerås, Sweden
{mojgann, owa, lhar, hansi}@kth.se

***Abstract*—The stacked polyphase bridges converter consists of several submodules that, on the input dc side, all are connected in series. Whereas controller designs presented in previous studies have been found promising for realizing equal voltage sharing between submodules, the survival and stability under fault conditions have not been studied. This paper presents a control strategy that enables survival of the converter after the occurrence of a sudden short circuit of a single transistor switch. The results are verified by simulations.**

I. Introduction

The advantages of modular converters have been exploited in high-voltage applications during the past decade [1]–[3]. This success has encouraged researchers to investigate these types of converters in medium-voltage or even low-voltage applications. Investigations have been carried out considering quite a wide variety of applications, ranging from aerospace to low-voltage power supplies [4]–[9]. Electric vehicles (EVs) and hybrid electric vehicles (HEVs) are among the targets [10], [11]. The integration of modular converters with electric motors in EVs and HEVs is interesting, due to reduced cabling and electro-magnetic interference [12].

The stacked polyphase bridges (SPB) converter is a low-voltage modular converter that has been proposed recently [7]–[9], [13]. This topology offers a simple and convenient integration with a fractional-slot-concentrated-winding (FSCW) permanent-magnet synchronous motor suitable for automotive applications [14]. As illustrated in Fig. 1, the SPB converter consists of several submodules that are connected in series on the dc side. Each submodule consists of a two-level, three-phase converter that is connected to a set of three-phase windings of the motor. This converter structure allows the usage of low-voltage components such as metal-oxide semiconductor field-effect transistors (MOSFETs) utilizing a high switching frequency (up to around 100 kHz). This gives the opportunity to use a very small, low-voltage film, or perhaps ceramic, capacitor for each submodule.

In automotive applications, vehicle reliability and passenger safety have the highest level of attention. Although using low-voltage components in the design can be considered as an advantage, compared to a conventional converter, the number of components, such as switches, drivers, and dc-link capacitors, is increased. Therefore, high reliability of each

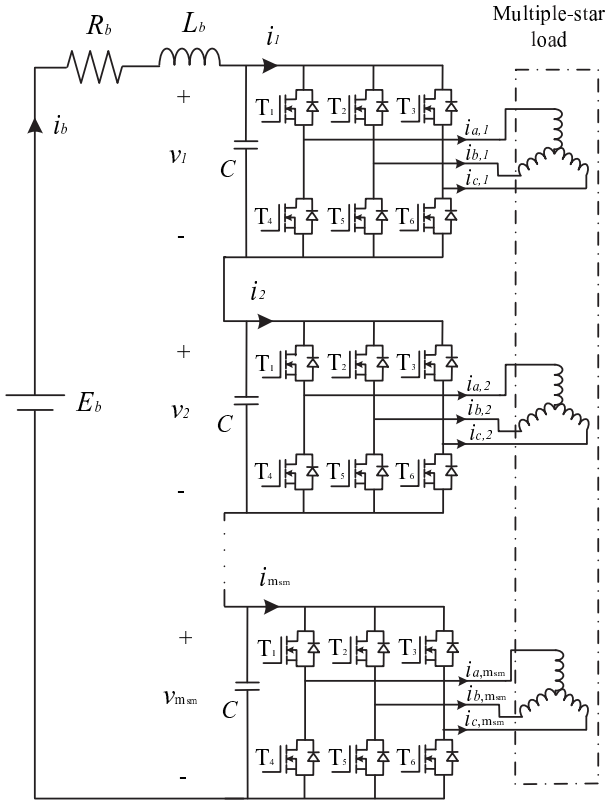

Fig. 1. The SPB converter topology with m_{sm} submodules.

of the components is very important. Even though previous studies show that MOSFETs and film capacitors have high reliability [15], [16], still, during the life time of the vehicle, there is a risk that a fault in any of these components might occur. Therefore, being able to survive a fault is important. As shown in Fig. 1, the number of MOSFETs is (at least) six times higher than the number of capacitors. Consequently, the fault risk for the MOSFETs is higher than for the film capacitors.

This paper presents a study considering the SPB converter when it faces a fault in one of the MOSFETs. A MOSFET fault means either a short circuit or an open circuit. The former fault type is considered here; the latter will be studied in

further research. In [17], a similar converter (for wind-turbine applications) during an unspecified submodule fault is studied. It is recommended that, in order to bypass the fault, a crowbar should be installed across each submodule. In addition, there is a circuit breaker for each phase of the submodule. However, such a fault handling strategy is not applicable for EVs and HEVs. Additional components are costly and consume space, which both are precious in automotive applications.

The objective of this paper is to investigate the possibility of a fault tolerant SPB converter without the addition of any extra components. In [18], the fault-tolerance capability of an FSCW motor connected to an SPB converter was investigated. It was verified that with a suitable motor design, when a short-circuit fault occurs at the motor terminals, the short-circuit current is less than the rated current. This motor design allows us to eliminate the breakers that are suggested in [17]. The control method proposed in this paper allows the faulty submodule to be bypassed without any crowbar. With this method, after the faulted MOSFET has been identified, in order to prevent a short circuit across the capacitor, the healthy MOSFET in the same phase leg is kept OFF. The MOSFETs in the remaining healthy phase legs are switched in a way that creates a short circuit across the motor windings that are connected to the faulty submodule. Due to that, the power into the windings goes to zero and there is no current flowing into the faulty submodule from the dc link. Therefore, the capacitor voltage of the faulty submodule will in motoring-mode operation increase momentarily. To discharge the capacitor, the operation should, as quickly as possible, be changed to generating mode. After discharging the capacitor safely, all the MOSFETs in the faulty submodule are turned ON, to create a short circuit across the capacitor without the usage of a crowbar.

The outline of paper is as follows. In Section II, the control system overview is presented. Fault analysis is studied in Section III. Simulation results are shown in Section IV. Finally, conclusions are drawn in Section IV.

II. Control System Overview

A model representing the capacitor-voltage dynamics for all submodules can be derived as follows. From Fig. 1, we have

$$L_b \frac{di_b}{dt} = E_b - R_b i_b - \sum_{k=1}^{m_{\text{sm}}} v_k, \tag{1}$$

where E_b, i_b, L_b, and R_b are voltage, current, inductance, and resistance of the voltage source (normally a battery), and v_k is the voltage across each submodule capacitor ($k = 1, 2, \ldots, m_{\text{sm}}$). All submodule capacitors are assumed to have the same capacitance C. For the kth capacitor voltage, with i_k as the current into the kth converter submodule, we have

$$C \frac{dv_k}{dt} = i_b - i_k. \tag{2}$$

The current i_k can be expressed as

$$i_k = \frac{P_k}{v_k}, \tag{3}$$

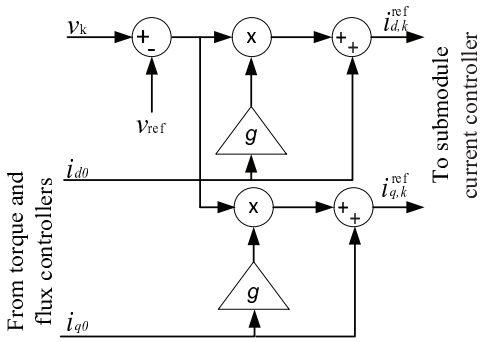

Fig. 2. Block diagram of the balancing controller.

where P_k is the power into the kth set of windings, assuming that the converter losses are negligible.

As found in [19], the dynamics of the submodule capacitor voltages are open-loop unstable in the motoring mode and need closed-loop stabilization. An individual stabilization term with a gain g can be added to the current-component references $i_{d,k}^{\text{ref}}$ and $i_{q,k}^{\text{ref}}$ for submodule k [19]. The stabilization terms for each submodule are made proportional to the individual voltage deviations from the reference voltage v_{ref}, as (see Fig. 2)

$$\begin{aligned} i_{d,k}^{\text{ref}} &= i_{d0} + g i_{d0}(v_k - v_{\text{ref}}) \\ i_{q,k}^{\text{ref}} &= i_{q0} + g i_{q0}(v_k - v_{\text{ref}}), \end{aligned} \tag{4}$$

where i_{d0} and i_{q0}, respectively, are set by the flux and torque controllers. These values are common for all submodules. Each submodule has a dedicated dq-frame current controller, with $i_{d,k}^{\text{ref}}$ and $i_{q,k}^{\text{ref}}$ as inputs along with locally obtained machine stator-current measurements. The current control loop has the bandwidth α_c. Local measurement of v_k, with minimal time delay, is used as well. Finally, the definition of v_{ref} is

$$v_{\text{ref}} = \begin{cases} v_\Sigma / m_{\text{sm}} & \text{for controller alternative I} \\ E_b / m_{\text{sm}} & \text{for controller alternative II} \\ v_{\Sigma f} / m_{\text{sm}} & \text{for controller alternative III} \end{cases} \tag{5}$$

where $v_\Sigma = \sum_{k=1}^{m_{\text{sm}}} v_k$ and $v_{\Sigma f}$ is a low-pass filtered variant of v_Σ. In the following, controller alternative I will be used.

III. Fault Analysis

Today, power electronics components are designed for high reliability. However, it is an unsafe assumption to consider these components as fault-free during the system life time.

In each submodule of the SPB converter, the diodes and the film capacitor tend to have a very high reliability [15]. MOSFETs are known as highly reliable components as well [16], yet a MOSFET fault should be more probable than a diode or capacitor fault. A MOSFET fault could happen as a short circuit or an open circuit. From now, we assume that a short-circuit fault has occurred in one of the MOSFETs in one submodule and this has been detected by its gate drive unit.

Assume, for example, that a short-circuit fault in MOSFET T_1 (see Fig. 1) in one submodule has been detected. If MOSFET T_4 in this situation is turned ON, a large current

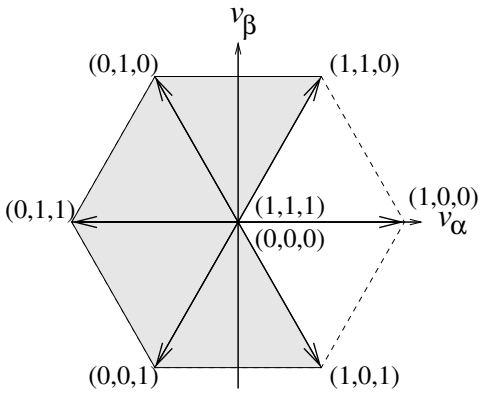

Fig. 3. Space-vector diagram for a short-circuit fault in MOSFET T_1 of one submodule.

spike through MOSFETs T_1 and T_4 will result due to the rapid discharge of the submodule capacitor. This causes a grave danger of an open-circuit fault in MOSFETs T_1 and/or T_4. Therefore, MOSFET T_4 should be kept OFF. The MOSFETs of the healthy phase legs, T_2/T_5 and T_3/T_6, can be switched ON/OFF [also denoted as (1)] or OFF/ON [also denoted as (0)]. Thereby, the switching vectors $(1,1,1)$, $(1,1,0)$, $(1,1,0)$, and $(1,0,1)$ can be created, see Fig. 3. Since only the two unshaded sectors can be accessed, v_α has always a dc bias and closed-loop current control can no longer be achieved. (If another MOSFET than T_1 has faced a short-circuit fault, then, similarly, a vector can always be created in two sectors that are next to each other.) Therefore, the best option is to short circuit the windings by applying the zero vector $(1,1,1)$ for a faulty upper MOSFET or $(0,0,0)$ for a faulty lower MOSFET.

When the short circuit is created by applying the vector $(1,1,1)$ or $(0,0,0)$, the resulting short-circuit current (in the dq frame) can be calculated from

$$L_d\frac{di_d}{dt} = v_d - R_s i_d + \omega_e L_q i_q \tag{6}$$

$$L_q\frac{di_q}{dt} = v_q - R_s i_q - \omega_e(L_d i_d + \psi_m) \tag{7}$$

where v_d and v_q are the stator voltage components ($v_d{=}v_q{=}0$), i_d and i_q are the stator current components, R_s is the stator resistance, ψ_m is the permanent-magnet flux linkage, ω_e is the angular rotor frequency, and L_d and L_q are the stator inductances.

The short-circuit current that results has typically a high transient peak and then settles to the steady-state values $i_d{=}-\psi_m/L_d$ and $i_q{=}0$, for a negligible stator resistance. Due to the (near) zero i_q, the torque production in the short-circuited windings is very small. To allow the steady-state operation under faulty conditions, the machine should be designed such that $|i_d|{=}\psi_m/L_d$ is smaller than the rated stator current [18], or the MOSFETs need to be overrated current wise.

Now, let us take a look at the submodule capacitor of the faulted submodule after the windings have been short circuited. The battery current i_b can no longer flow through the MOSFETs of the faulty submodule, it will instead flow through the submodule capacitor. If the machine was operating in the motoring mode before the occurrence of the fault, then the voltage of the faulty submodule's capacitor will increase. It is important to stop this voltage increase as soon as possible, because overvoltage across the submodule capacitor may damage the capacitor and/or the MOSFETs. Therefore, the control system needs to eliminate this problem by temporarily changing the operation mode from motoring to generating until the capacitor is completely discharged. The capacitor should have a capacitance large enough to prevent the voltage from rising to a dangerously high level during the time needed for the control system to change the mode of operation (typically in the range of milliseconds).

In the final step, the control system safely creates a short circuit across the faulty submodule by turning ON all the healthy MOSFETs. Now, the motoring-mode operation can resume. It is important to avoid overcurrent in the MOSFETs of the faulty submodule. For this reason, the power of each healthy submodule may need to be limited to a value less than the nominal power in order to keep i_b sufficiently low. The two MOSFETs in each phase leg of the faulty submodule are both turned ON. Consequently, current with direction into the winding will be conducted in the upper MOSFET, whereas current with direction out of the winding will be conducted in the lower MOSFET. Assuming for simplicity that the phase current is sinusoidal, one period of the MOSFET current—for either one of the two MOSFETs in one phase leg—can be expressed as

$$i_M = \begin{cases} \frac{i_b}{3} + \frac{\psi_m}{L_d}\sin(\omega_e t), & 0 \le t < \frac{T}{2} \\ \frac{i_b}{3}, & \frac{T}{2} \le t < T \end{cases} \tag{8}$$

where $T = 2\pi/\omega_e$ and it is assumed that peak-value space-vector scaling is used. Clearly, the peak value of i_M is given by

$$\hat{I}_M = \frac{i_b}{3} + \frac{\psi_m}{L_d}, \tag{9}$$

whereas the rms value can be calculated as

$$I_M = \sqrt{\frac{1}{T}\int_0^T i_M^2\, dt}. \tag{10}$$

Substituting the expression of (8) into (10) gives

$$I_M = \sqrt{\frac{i_b^2}{9} + \frac{2\psi_m i_b}{3\pi L_d} + \frac{\psi_m^2}{4L_d^2}}. \tag{11}$$

The current i_b needs to be small enough such that neither (9) nor (11) exceeds the rated value for the MOSFET used.

IV. Simulation Results

This section presents simulation results for an SPB converter connected to an FSCW machine. The data for the converter and the machine are presented in Table IV. They are similar but not identical to those found in [18], [19].

A short-circuit fault occurring at $t = 0$ in one of the MOSFETs of submodule 4 is simulated. Immediately before

TABLE I
CONVERTER AND MACHINE DATA

Converter parameters			
m_{sm}	4	—	number of submodules
E_b	400	V	source voltage
$v_{1,2,\ldots,m_{\text{sm}}}$	100	V	voltages at no-load operation
C	100	μF	submodule capacitance
L_b	8.0	μH	source inductance
R_b	32	mΩ	source resistance
f_{sw}	20	kHz	switching frequency
Machine parameters			
P_{nom}	7.4	kW	rated power per submodule
I_s	130	A	rated rms current per submodule
R_s	4.3	mΩ	stator resistance per submodule
L_d	10.3	μH	d-direction inductance per submodule
L_q	18.8	μH	q-direction inductance per submodule
ψ_m	0.020	Vs	flux linkage per submodule
n_p	4	—	number of pole pairs
ω_e	1.42	krad/s	angular freq. at rated speed 3400 rpm
α_c	22	krad/s	bandwidth of current control loop
T_d	0.1	ms	submodules communication time delay

the fault, the motor is running at the rated speed (3400 rpm), the rated current ($i_d = 0, i_q = 184$ A), and the rated power (7.4 kW) per submodule. Ideally, for $R_b = 0$, the battery current would be given by $i_b = m_{\text{sm}} P_{\text{nom}}/E_b = 74$ A, whereas in the simulation it is 82 A due to the losses (see Fig. 5). Immediately after the fault occurrence at $t = 0$, the motor windings that are connected to the faulty submodule are short circuited. In Fig. 4, the short-circuit current components and their modulus are shown. As can be seen, the maximum peak value is approximately 550 A during the transient. The current then settles to $\psi_m/L_d = 200$ A, which is 16 A higher than the rated current.

At the same time (at $t = 0$), the capacitor voltage of the faulty submodule starts to increase, because the battery current starts flowing through the capacitor instead of the faulty converter (note in Fig. 5(c) that i_4 immediately goes to zero after the fault occurrence). The healthy submodule capacitor voltages simultaneously start to decrease and consequently, due to the stabilization controller, their phase currents increase slightly. This can be observed as increases of $i_{1,2,3}$.

At $t = 0.1$ ms, when the time delay T_d has passed, the submodule controllers recognize that one submodule is faulty and the number of submodules is changed as $m_{\text{sm}} \to m_{\text{sm}} - 1 = 3$ in (5). In order to discharge the capacitor of the faulty submodule safely, the submodule controllers put the machine in the generating mode with $i_q^{\text{ref}} = 100$ A (this value is just an example). This makes i_b negative (see Fig. 5(a)).

After the capacitor of the faulty submodule is discharged completely, all the MOSFETs in the faulty submodule are turned ON to create a short circuit across the capacitor. Simultaneously, the controllers of the healthy submodules put the machine in the motoring mode again. As a result, the battery current increases, but settles at a value lower than before the fault occurrence, $i_b = 46$ A. The reason is that, after dropping one submodule the voltage across each healthy

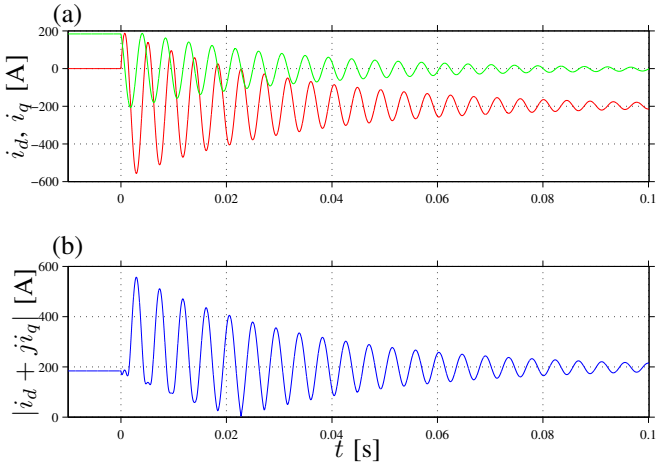

Fig. 4. A short-circuit fault on T_1 of submodule 4: (a) Current components. (b) Current modulus.

submodule increases to approximately $E_b/(m_{\text{sm}} - 1) = 133$ V. From (9), the steady-state peak current in each MOSFET of the faulty submodule is obtained as 213 A, which is 29 A higher than in the healthy situation.

Remark: In [19], the communication time delay was approximately 0.5 ms, which is too long for this strategy to work. As can be seen in Fig. 5(b), at $t = 0.5$ ms, the capacitor voltage would have charged to an unacceptably high value. On the other hand, a time delay much smaller than 0.1 ms would make the peak capacitor voltage across the faulty submodule significantly smaller than the 180 V shown in Fig. 5(b).

V. CONCLUSION

This paper presents a control strategy for the SPB converter to enable its survival under a sudden transistor short-circuit fault. The proposed control method allows bypassing the faulty submodule without using additional devices such as breakers or crowbars. After recognizing the faulty MOSFET, the other MOSFET in the same phase leg is kept OFF and other healthy MOSFETs in the other phase legs in the same submodule are switched in a way to create a short circuit across the motor winding. Subsequently, the controllers of the healthy submodules put the machine in the generating mode as quickly as possible to discharge safely the capacitor voltage of the faulty submodule. After discharging the capacitor voltage completely, all MOSFETs in the faulty submodule are switched ON to create a short circuit across the capacitor. Thereafter, the controllers of the healthy submodules resume the motoring mode for the machine. Now, the SPB converter can operate normally with one submodule less. All the results regarding this control strategy were verified through simulations.

ACKNOWLEDGMENT

The authors gratefully acknowledge the Swedish Hybrid Vehicle Centre (SHC) for the financial support.

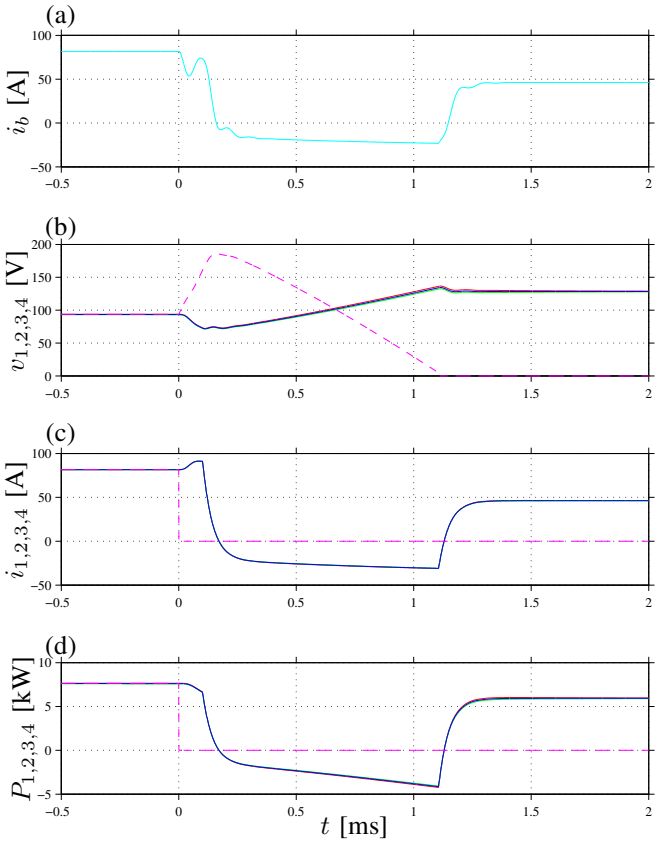

Fig. 5. A short-circuit fault on T_1 of submodule 4: (a) Current drawn from the voltage source (e.g., battery). (b) Capacitor voltage for the kth submodule; red, green, blue, and magenta respectively for $k=1,2,3,4$. (c) Current into the kth submodule; red, green, blue, and magenta respectively for $k=1,2,3,4$. (d) Power into the kth set of windings; red, green, blue, and magenta respectively for $k=1,2,3,4$.

REFERENCES

[1] L. G. Franquelo, J. Rodriguez, J. I. Leon, S. Kouro, R. Portillo, and M. A. M. Prats, "The age of multilevel converters arrives," *IEEE Industrial Electronics Magazine*, vol. 2, no. 2, pp. 28–39, Jun. 2008.

[2] J. Rodriguez, S. Bernet, B. Wu, J. Pontt, and S. Kouro, "Multilevel voltage-source-converter topologies for industrial medium-voltage drives," *IEEE Transactions on Industrial Electronics*, vol. 54, no. 6, pp. 2930–2945, Dec. 2007.

[3] N. Flourentzou, V. G. Agelidis, and G. D. Demetriades, "VSC-based HVDC power transmission systems: An overview," *IEEE Transactions on Power Electronics*, vol. 24, no. 3, pp. 592–602, Mar. 2009.

[4] M. Gleissner and M. M. Bakran, "Reliable fault-tolerant DC/DC-converter structures," in *Proceedings of International Exhibition and Conference for Power Electronics, Intelligent Motion, Renewable Energy and Energy Management (PCIM Europe 2014)*, May 2014, pp. 1–8.

[5] R. H. Williams, D. A. Stone, M. P. Foster, and S. R. Minshull, "Reduction of passive filtering in aerospace starter/generator systems using a multilevel converter with predictive current control," in *Proceedings of the 6th IET International Conference on Power Electronics, Machines and Drives (PEMD 2012)*, Mar. 2012, pp. 1–5.

[6] M. S. Bhaskar, N. Sreeramula Reddy, R. K. P. Kumar, and Y. B. S. S. Gupta, "A novel high step-up multilevel boost converter using double voltage-lift switched-inductor cell," in *Proceedings of International Conference on Circuit, Power and Computing Technologies (ICCPCT 2014)*, Mar. 2014, pp. 996–1001.

[7] S. Gjerde and T. Undeland, "Power conversion system for transformerless offshore wind turbine," in *Proceedings of the 14th European Conference on Power Electronics and Applications (EPE 2011)*, Aug. 2011.

[8] S. Gjerde, P. Olsen, K. Ljokelsoy, and T. Undeland, "Control and fault handling in a modular series-connected converter for a transformerless 100 kV low-weight offshore wind turbine," *IEEE Transactions on Industry Applications*, vol. 50, no. 2, pp. 1094–1105, Mar. 2014.

[9] Y. Han, "Design, modeling, and control of multilevel converter motor drive with modular design and split winding machine," in *Proceedings of the IEEE 15th Workshop on Control and Modeling for Power Electronics (COMPEL 2014)*, Jun. 2014.

[10] N. McNeill, X. Yuan, and P. Anthony, "High-efficiency multilevel converter technology for electric vehicle applications using super-junction MOSFETs," in *Proceedings of the 5th IET Hybrid and Electric Vehicles Conference (HEVC 2014)*, Nov. 2014, pp. 1–7.

[11] L. Lambertz, R. Marquardt, and A. Mayer, "Modular converter systems for vehicle applications," in *Emobility – Electrical Power Train, 2010*, Nov. 2010, pp. 1–6.

[12] M. Schier, F. Rinderknecht, and N. S. Kumar, "Highly integrated electric drives for automotive application," in *Proceedings of International Conference on Sustainable Mobility Applications, Renewables and Technology (SMART 2015)*, Nov. 2015, pp. 1–6.

[13] S. Norrga, L. Jin, O. Wallmark, A. Mayer, and K. Ilves, "A novel inverter topology for compact EV and HEV drive systems," in *Proceedings of the IEEE 39th Annual Conference Industrial Electronics Society, (IECON 2013)*, Nov. 2013, pp. 6590–6595.

[14] H. Zhang, O. Wallmark, M. Leksell, S. Norrga, M. Harnefors, and L. Jin, "Machine design considerations for an MHF/SPB-converter based electric drive," in *Proceedings of the IEEE 40th Annual Conference Industrial Electronics Society, (IECON 2014)*, Oct. 2014, pp. 3849–3854.

[15] H. Wang and F. Blaabjerg, "Reliability of capacitors for DC-link applications in power electronic converters: An overview," *IEEE Transactions on Industry Applications*, vol. 50, no. 5, pp. 3569–3578, Sep. 2014.

[16] S. Yang, D. Xiang, A. Bryant, P. Mawby, L. Ran, and P. Tavner, "Condition monitoring for device reliability in power electronic converters: A review," *IEEE Transactions on Power Electronics*, vol. 25, no. 11, pp. 2734–2752, Nov. 2010.

[17] S. Gjerde and T. M. Undeland, "Fault tolerance of a 10 MW, 100 kV transformerless offshore wind turbine concept with a modular converter system," in *Proceedings of the 15th International Power Electronics and Motion Control Conference (EPE/PEMC, 2012)*, Sep. 2012, pp. LS7c.3–1–LS7c.3–8.

[18] H. Zhang, O. Wallmark, and M. Leksell, "On fault tolerance for IPM-FSCW machines adopting a modular converter," in *Proceedings of the 17th International Conference on Electrical Machines and Systems (ICEMS, 2014)*, Oct. 2014, pp. 1633–1638.

[19] M. Nikouie, O. Wallmark, L. Jin, L. Harnefors, and H.-P. Nee, "DC-link stability analysis and controller design for the stacked polyphase bridges converter," *IEEE Transactions on Power Electronics*, accepted for publication.